Nonequilibrium Josephson effect in short-arm diffusive SNS interferometers

E. V. Bezuglyi
B. Verkin Institute for Low Temperature Physics and Engineering, Kharkov 61103, Ukraine

V. S. Shumeiko and G. Wendin
Chalmers University of Technology and Göteborg University, S-41296 Göteborg, Sweden

(Received 20 March 2003; revised manuscript received 21 April 2003; published 6 October 2003)

We study nonequilibrium Josephson effect and phase-dependent conductance in three-terminal diffusive interferometers with short arms. We consider strong proximity effect and investigate an interplay of dissipative and Josephson currents coexisting within the same proximity region. In junctions with transparent interfaces, the suppression of the Josephson current appears at rather large voltage, $eV \sim \Delta$, and the current vanishes at $eV \geqslant \Delta$. Josephson current inversion becomes possible in junctions with resistive interfaces, where it occurs within a finite interval of the applied voltage. Due to the presence of considerably large and phase-dependent injection current, the critical current measured in a current biased junction does not coincide with the maximum Josephson current, and remains finite when the true Josephson current is suppressed. The voltage dependence of the conductance shows two pronounced peaks, at the bulk gap energy and at the proximity gap energy; the phase oscillation of the conductance exhibits qualitatively different form at small voltage $eV < \Delta$, and at large voltage $eV > \Delta$.

DOI: 10.1103/PhysRevB.68.134506 PACS number(s): 74.25.Fy, 74.45.+c, 73.23.−b

I. INTRODUCTION

Multiterminal superconductor–normal-metal–superconductor (SNS) junctions are interesting devices where an interplay between the dissipative normal electron current and nondissipative Josephson current can be studied. The simplest device of this type consists of two superconducting reservoirs and one normal reservoir connected by a small normally conducting T-shaped bridge, see Fig. 1(a). A mesoscopic size of the bridge is essential to keep the coherence of the current transport over the whole device. During the last decade, a large amount of interesting experiments have been done with such kind of devices (for the review see Ref. 1 and references therein, further references can be found in Ref. 2).

Nonequilibrium state in multiterminal SNS junctions exhibits two closely related major phenomena: the interferometer effect, which concerns the dependence of normal conductance of the device on the phase difference between the superconducting reservoirs,[3] and the Josephson transistor effect, which concerns the dependence of the Josephson current on the current injected from the normal reservoir.[4,5] The interferometer effect gives rise to a number of so-called Josephson-like effects.[6,7]

The interferometer effect has received most of the attentions; it has been extensively studied experimentally[8,1] and theoretically,[9,1,2] and presently, this effect is rather well understood. The proximity of the superconducting reservoirs leads to a modification of the density of states and transport properties of the normal bridge (proximity effect), which therefore become sensitive to the phase difference at the reservoirs, and exhibit oscillating behavior as the function of the phase difference.

The Josephson transistor effect has been also observed in experiment.[10–12] The nonequilibrium Josephson effect has been first predicted[4] and then theoretically studied in the ballistic junctions.[13–15,2] Nonequilibrium population of the Andreev states[16] induced by the current injection leads to a full-scale variation of the Josephson current with the applied voltage and to the inversion of the current direction. Similar transistor effect has been also investigated in diffusive junctions.[17–20]

Most of the experiments with multiterminal junctions have been done using diffusive metallic bridges, whose length was large compared to the superconducting coherence length ξ_0. In such long junctions, the proximity effect is suppressed, which results in small amplitude of the conductance oscillation (typically few percents of the full conductance value), and small magnitude of the Josephson current. In theoretical analysis of the interferometer effect in diffusive junctions, the presence of the Josephson current is usually ignored. Similarly, the theoretical studies of the nonequilibrium Josephson effect[17–19] are restricted to the regime of ''weak'' proximity effect,[9,21,22] when the induced gap in the normal bridge is much smaller than those in the supercon-

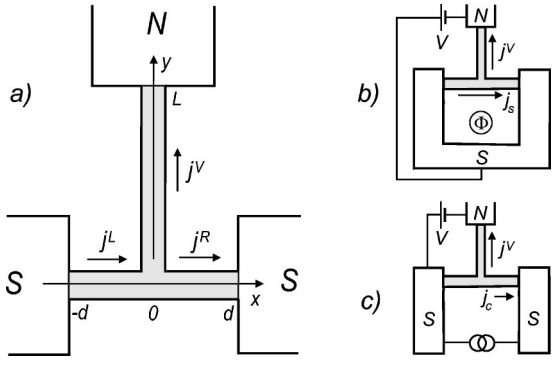

FIG. 1. Sketch of three-terminal SNS interferometer: T-shape diffusive metallic wire with short arms (shaded region) is connected to superconducting (S) and normal (N) reservoirs (a), flux bias setup for measuring current-phase relation (b), and current bias setup for measuring critical current (c).

ducting reservoirs. Such a regime is relevant for long diffusive junctions and for junctions with high-resistance NS interfaces. In addition, the nonequilibrium Josephson current was calculated for specific four-terminal circuit geometries where the dissipative normal current and the Josephson current were spatially separated.

Meanwhile, it is conceptually interesting to investigate the problem of interplay of dissipative and Josephson currents flowing in the same diffusive lead under a strong proximity effect. In this paper, we address this problem by studying the nonequilibrium Josephson effect in three-terminal SNS interferometers with short arms, whose lengths are *smaller* than the coherence length ξ_0.

Coexistence of dissipative and nondissipative currents in the same proximity region makes it difficult to identify the Josephson current component. In equilibrium, the total current flowing through a proximity lead is the Josephson current, which is entirely determined by the supercurrent spectral density and the population numbers of the relevant states. The presence of the normal injection current and related gradients of the distribution functions violates the local conservation of the supercurrent component which varies along the lead, and hence its direct connection to the Josephson current is lost. Nevertheless, as we will show in the paper, a simple picture of the nonequilibrium Josephson effect as the result of nonequilibrium population of the states with the same current spectral density as in equilibrium can be justified for some particular cases (see also Ref. 12). However, a general situation seems to be more complex.

In the short-arm SNS interferometers, the proximity effect is strong when the interfaces are transparent, but it also may be strong when the interfaces are highly resistive. The measure of the strength of the proximity effect is the magnitude of the induced energy gap, which is comparable with the superconducting energy gap in the reservoirs. Consequently, there are full-scale variations of the Josephson current and the normal conductance with the applied voltage and the phase difference.

In short diffusive junctions with transparent interfaces, the Josephson current is solely carried by the Andreev states whose energies are smaller than the superconducting energy gap, which is similar to the short ballistic junctions.[23,5] Consequently, in these junctions, the Josephson current can be suppressed to zero but never be reversed. The Josephson current reversion becomes possible in the junctions with resistive interfaces due to the negative contribution of the states with energies above the bulk energy gap. Moreover, in contrast to weak proximity regime,[17] the current reversion exhibits a fine structure similar to the one theoretically discussed for ballistic junctions,[15] and recently demonstrated in the experiment with long diffusive junctions.[11]

The interplay of the injected and Josephson currents in the strong proximity regime is important for the interpretation of experiments with current biased junctions, Fig. 1(c). The magnitude of the nonequilibrium critical Josephson current measured with this setup is different, as we will show, from the one derived from the current-phase relation measured by an rf superconducting quantum interference device (SQUID), Fig. 1(b). This phenomenon has been earlier noticed in the absence of true Josephson current in the weak proximity regime.[6]

The structure of the paper is the following. After introducing a basic formalism in Sec. II, we discuss the spectral functions in Sec. III, and the distribution functions in Sec. IV. Sections V and VI are devoted to a discussion of the nonequilibrium Josephson effect; the interferometer effect is considered in Sec. VII.

II. BASIC EQUATIONS

The junction we are going to investigate is sketched in Fig. 1(a). It consists of two superconducting reservoirs and a normal reservoir connected by mesoscopic T-shape diffusive metallic bridge. Such a geometry can be realized in experiment, e.g., by using nanowire technology.[24] The superconducting reservoirs are assumed to have equal potentials, and the superconducting phase difference between the reservoirs is ϕ. The distance between the superconductors, $2d$ ($-d<x<d$), and the length of the injection lead, L ($0<y<L$), are assumed to be small compared to the superconducting coherence length $\xi_0=\sqrt{\hbar\mathcal{D}/\Delta}$ ($\mathcal{D}$ is the diffusion coefficient), however, the relation between these lengths can be arbitrary. For simplicity, we assume the cross sections and normal conductivities of all wires to be equal, and the current from the voltage-biased normal reservoir to be injected in the middle of the SNS junction.

Neglecting spatial variations of all quantities across the leads, we use one-dimensional static equations[25] for the 4×4 matrix Keldysh-Green's function $\check{G}$ in the normal leads, in which we neglect the inelastic collision term

$$[\sigma_z E,\check{G}]=i\hbar\mathcal{D}\partial\check{J},\quad \check{J}=\check{G}\partial\check{G},\quad \check{G}^2=\check{1}, \tag{1}$$

$$\check{G}=\begin{pmatrix}\hat{g}^R & \hat{G}^K\\ 0 & \hat{g}^A\end{pmatrix},\quad \hat{G}^K=\hat{g}^R\hat{f}-\hat{f}\hat{g}^A. \tag{2}$$

Here $\hat{g}^{R,A}$ are the retarded and advanced Green's functions, $\hat{f}=f_+ +\sigma_z f_-$ is the matrix distribution function, and ∂ denotes spatial derivative. At the junction node, the matrix current $\check{J}$ obeys the Kirchhoff's rule[26]

$$\check{J}_{x=-0}=\check{J}_{x=+0}+\check{J}_{y=+0}. \tag{3}$$

The Keldysh component $\hat{J}^K$ of the matrix current $\check{J}$ determines the electric currents in the leads,

$$j=\frac{\sigma}{4e}\int_0^\infty dE\,\mathrm{Tr}\,\sigma_z\hat{J}^K=\frac{\sigma}{e}\int_0^\infty dE\,I_-(E), \tag{4}$$

where σ is the normal conductivity. The current spectral density $I_-(E)$ in Eq. (4) has three components,[22]

$$I_-\equiv(1/4)\mathrm{Tr}\,\sigma_z\hat{J}^K=D_-\partial f_- +I_s f_+ -I_{an}\partial f_+. \tag{5}$$

The first term in Eq. (5) describes a dissipative current which provides usual Drude conductivity in the normal state. The second term gives conventional Josephson current in equilib-

rium, while the third term, the anomalous current,[22] appears in nonequilibrium superconducting junctions. Another diagonal component of $\hat{J}^K$,

$$I_+ \equiv (1/4)\mathrm{Tr}\,\hat{J}^K = D_+\partial f_+ + I_s f_- + I_{an}\partial f_-, \qquad (6)$$

has the meaning of the net quasiparticle current (the sum of the electron and hole probability currents). Explicit equations for the spectral characteristics of the junction, $D_\pm$, I_s, and I_{an}, are conveniently written in terms of the following parametrization of the matrix $\hat{g}$:

$$\hat{g} = \hat{u} + \hat{v} = \sigma_z u + \exp(i\sigma_z\psi) i\sigma_y v, \quad u^2 - v^2 = 1. \qquad (7)$$

The function u is related to the quasiparticle density of states (DOS), normalized by its value in the normal state, $N(E,x) = \mathrm{Re}\,u^R(E,x)$, while the function v is related to the spectral density of the condensate. The complex phase ψ appears in the presence of a supercurrent. In these notations, the diffusion coefficients read

$$D_\pm = (1/4)\mathrm{Tr}(1 - \hat{u}^R\hat{u}^A \mp \hat{v}^R\hat{v}^A) = (1/2)[1 + |u^R|^2 \mp |v^R|^2\cosh(2\,\mathrm{Im}\,\psi^R)]. \qquad (8)$$

In the normal state, $D_\pm$ turn to unity.

The spectral densities of the supercurrent and anomalous current are given by the equations

$$I_s = (1/4)\mathrm{Tr}\,\sigma_z(\hat{v}^R\partial\hat{v}^R - \hat{v}^A\partial\hat{v}^A) = -\mathrm{Im}(v^2\partial\psi)^R, \qquad (9a)$$

$$I_{an} = (1/4)\mathrm{Tr}\,\sigma_z\hat{v}^R\hat{v}^A = -|v^R|^2\sinh(2\,\mathrm{Im}\,\psi^R)/2. \qquad (9b)$$

In Eqs. (8) and (9), the relations $(u,v)^A = -(u,v)^{R*}$ and $\psi^A = \psi^{R*}$ are used, which follow from the general relationship $\hat{g}^A = -\sigma_z\hat{g}^{R\dagger}\sigma_z$.[25]

Calculation of the electric current in Eq. (4) involves the two steps: first one has to solve the Usadel equations for the Green's functions $\hat{g}^{R,A}$, and then to solve the kinetic equations to find the distribution functions.

III. SPECTRAL FUNCTIONS

The Green's function components of Eq. (1) represent the Usadel equations for the spectral functions,[27]

$$2Ev = i\hbar\mathcal{D}[\partial(u\partial v - v\partial u) - uv(\partial\psi)^2], \qquad (10)$$

$$v^2\partial\psi = I, \qquad (11)$$

where the spatial constant $I(E)$ is related to the supercurrent spectral density in Eq. (9), $I_s = -\mathrm{Im}\,I^R$. In terms of the spectral angle θ related to the spectral functions as $u = \cosh\theta$, $v = \sinh\theta$, Eq. (10) takes the form

$$\partial^2\theta = (2E/i\hbar\mathcal{D})\sinh\theta + I^2\cosh\theta/\sinh^3\theta. \qquad (12)$$

The two terms on the right-hand side (rhs) of Eq. (12) are related to two different depairing mechanisms, which provide spatial decrease of θ towards the middle of the junction. The first term is associated with the dephasing between the electron and hole wave functions at finite energy E. The second term describes depairing caused by the time-reversal symmetry breaking due to supercurrent flow.

The solution of Eqs. (11) and (12) reads

$$x_i = \int_{\theta_0}^{\theta(E,x_i)} \frac{d\theta}{\sqrt{R(E,\theta)}}, \quad x_i = x,y, \qquad (13)$$

$$\psi(E,x_i) = \psi_0 + I\int_0^{x_i}\frac{dz}{v^2(E,z)}, \qquad (14)$$

$$R(E,\theta) \equiv C + (4E/i\hbar\mathcal{D})\cosh\theta - (I/\sinh\theta)^2, \qquad (15)$$

where $C(E)$ is the integration constant, and θ_0 and ψ_0 are the spectral functions at the junction node. The boundary conditions for Eqs. (11) and (12) are imposed by the conservation law for the matrix current in Eq. (3),

$$\partial_x\theta|_{x=-0} = \partial_x\theta|_{x=+0} + \partial_y\theta|_{y=0}, \qquad (16)$$

and similar equation for the function ψ. At the normal electrode, the current I turns to zero, which means that $I \equiv 0$ along the injection lead, and therefore $\psi(y) \equiv \mathrm{const}$. Hence, the derivative of ψ is continuous in the horizontal lead, whereas $\theta(x)$ has a kink at $x = 0$. In what follows, we consider symmetric junction, in which $\theta(x)$ is even, and $\psi(x)$ is odd function. In this case, the phase ψ, together with the anomalous current I_{an}, turns to zero at the junction node, and the kink in $\theta(x)$ is symmetric, $\theta_0' \equiv \partial_x\theta|_{x=+0} = -\partial_x\theta|_{x=-0}$.

The boundary conditions at the NS interfaces depend on the interface resistance. Below we analyze the two different situations related to perfect and high-resistive interfaces, respectively.

A. Transparent interfaces

If the interface electric resistance R_{NS} is much smaller than the normal resistance R_N of the horizontal lead, one can assume the spectral functions to be continuous at $x = \pm d$, namely, $\psi(\pm d) = \pm\phi/2$ and $\theta(\pm d) = \theta_S \equiv \mathrm{arctanh}(\Delta/E)$; at the normal electrode $\theta = 0$. In this limit, the second term in the rhs of Eq. (15) can be neglected due to large gradients of the spectral functions along the leads, which results in linear change of θ along the injection lead, $\theta(E,y) = \theta_0(1 - y/L)$, and the boundary condition in Eq. (16) takes the form

$$\theta_0 = 2\theta_0' L. \qquad (17)$$

The analytical expressions for the spectral functions in the horizontal lead within this approximation have been found in Ref. 20. In the right lead, they are given by

$$u(E,x) = \tilde{u}_0\cosh(\alpha + \Lambda x/d), \qquad (18)$$

$$\psi(E,x) = \arctan[\tilde{v}_0^{-1}\tanh(\alpha + \Lambda x/d)] - p. \qquad (19)$$

The solution in the left lead is obtained by the change of the signs of x, ϕ, α, and p. The spatial constants in Eqs. (18) and (19) can be parametrized as

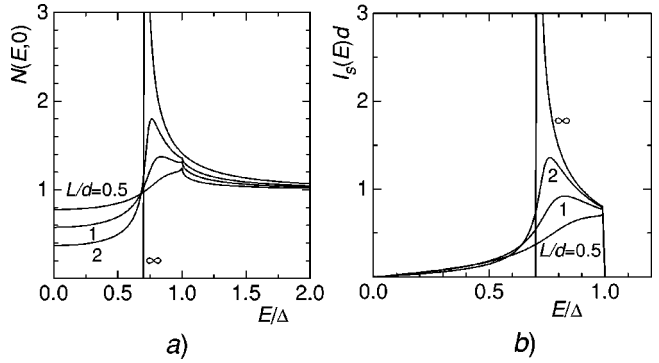

FIG. 2. The density of states, $N(E,0)$, at the device node (a), and the supercurrent spectral density $I_s(E)$ at $\phi=\pi/2$ (b), at several values of the ratio L/d, calculated by using numerical solution of Eq. (23).

$$I=\frac{\tilde{v}_0}{d}\Lambda, \quad \Lambda=\operatorname{arccosh}\frac{u_S}{\tilde{u}_0}-\operatorname{arccosh}\frac{u_0}{\tilde{u}_0}, \tag{20}$$

$$u_0\equiv\cosh\theta_0=\tilde{u}_0\cosh\alpha=u_S(\tilde{E},\tilde{\Delta}), \tag{21}$$

$$\tilde{u}_0=u_S(E,\tilde{\Delta}), \quad \tilde{E}=E\cos p, \quad \tilde{\Delta}=\Delta\cos(\phi/2+p), \tag{22}$$

where $u_S(E,\Delta)=E/\sqrt{E^2-\Delta^2}$, and expressed via a single parameter p, which is to be evaluated from the equation following from Eq. (17),

$$\tilde{u}_0\Lambda\sin p=a\theta_0. \tag{23}$$

The magnitude of the parameter p is controlled by the parameter $a=d/2L$. When a decreases, i.e., the resistance of the injection lead increases, p turns to zero, according to Eq. (23), and the spectral functions approach their values in closed short SNS junctions. In the limit $a=0$, DOS has the proximity gap $|\Delta_\phi|$, where $\Delta_\phi=\Delta\cos(\phi/2)$, and reveals a BCS-like singularity at the gap edge,

$$N(E,0)=E\Theta(E-|\Delta_\phi|)/\sqrt{E^2-\Delta_\phi^2}, \tag{24}$$

where $\Theta(x)$ is the Heaviside step function. The supercurrent spectral density $I_s(E)$ spreads over the region $|\Delta_\phi|\leqslant E\leqslant\Delta$, and has the singularity at the proximity gap edge as well,[28]

$$I_s(E)=\frac{\pi}{2d}\frac{\Delta_\phi\Theta(E-|\Delta_\phi|)}{\sqrt{E^2-\Delta_\phi^2}}\Theta(\Delta-E). \tag{25}$$

In a general case, $a\neq0$, the proximity of the normal reservoir leads to finite DOS at all energies, as shown in Fig. 2(a), though it is noticeably suppressed at $E<|\Delta_\phi|$ for $L\gtrsim d$. The supercurrent spectral density at finite d/L extends over the whole subgap region [see Fig. 2(b)], while at $E>\Delta$, both I_s and I_{an} turn to zero. Thus, in short diffusive junctions with transparent interfaces, the supercurrent is carried exclusively by the bound Andreev states confined to the potential well formed by the junction. However, this result is only correct to zero approximation with respect to the small parameter d/ξ_0.[29]

B. Opaque interfaces

The effect of the interface becomes important when the interface resistance R_{NS} exceeds the resistance of the normal conductor $R_N=2d/\sigma$, $r=R_{NS}/R_N\gg1$. In particular, the magnitude of the Josephson current is determined by the R_{NS} rather than by R_N in the limit $r\gg1$. At the same time, as we will see below, the suppression of the proximity effect is governed by much smaller parameter $r(d/\xi_0)^2\ll r$, and the proximity effect can be strong even when $r\gg1$.

A high-resistive interface can be modeled by an effective tunnel barrier characterized by its resistance R_{NS} in the normal state, which results in the following boundary conditions for the Green's functions[30] at $x=d$:

$$\sigma R_{NS}\partial\theta_N=u_Nv_S\cos(\phi/2-\psi_N)-u_Sv_N, \tag{26a}$$

$$\sigma R_{NS}I=v_Nv_S\sin(\phi/2-\psi_N), \quad I=v_N^2\partial\psi_N, \tag{26b}$$

and similar for $x=-d$ (the indices N and S refer to the normal and superconducting sides of the interface).

In the limit $r\gg1$, the spatial variation of the spectral phase is strongly nonhomogeneous: the phase drops at the barriers and is small in the normal region, $\psi_N\ll1$, along with the spectral current I. The spatial variation of the spectral function u is small and can be approximated by a weakly varying parabolic function,

$$u(E,x)\approx u_0[1+(\beta/2)(x/d)^2]. \tag{27}$$

In Eq. (27), we neglected the effect of the injection lead, assuming its resistance to be larger than R_{NS}, $1/a\gg r$. The coefficient $\beta\ll1$ is to be found from Eq. (15), in which the electron-hole dephasing effect has to be taken into account because it now becomes comparable with the small current-induced depairing,

$$\beta=-2i\frac{E}{\Delta}\left(\frac{d}{\xi_0}\right)^2\frac{v_0^2}{u_0}+\left(\frac{Id}{v_0}\right)^2. \tag{28}$$

In Eq. (14), we may neglect spatial variations of the integrand which results in a linear spatial dependence of the phase, $\psi(E,x)\approx Ix/v_0^2\sim r^{-1}$.

By making use of Eqs. (27) and (28), the boundary conditions in Eqs. (26) give the equation for the spectral functions u_N and v_N,

$$\frac{u_S}{u_N}=\frac{i\gamma E}{u_N\Delta}+\frac{v_S}{v_N}\cos\frac{\phi}{2}-r\psi_N^2, \quad \gamma=2r(d/\xi_0)^2, \tag{29}$$

and the expression for the spectral current I,

$$I=\frac{v_Nv_S}{\sigma R_{NS}}\sin\frac{\phi}{2}, \tag{30}$$

in which we omitted the small phase ψ_N from the trigonometric functions. Equation (29) describes three mechanisms of depairing. The first term in the rhs represents the electron-

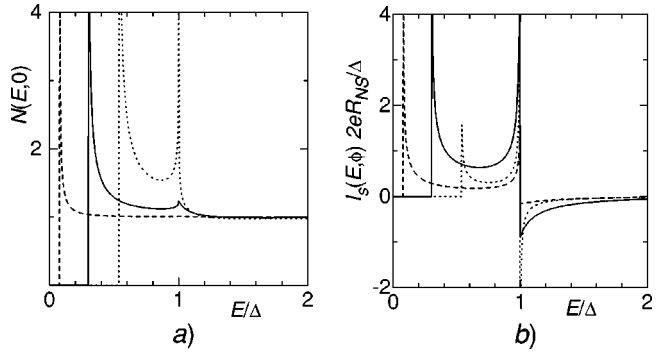

FIG. 3. Variations in the density of states (a), and in the supercurrent spectral density (b) with the phase difference in SINIS junction, calculated from Eqs. (31) and (32) at $\gamma=1$: $\phi=0.1\pi$ (dotted lines), 0.6π (solid lines), and 0.9π (dashed lines).

hole dephasing within the normal metal. The parameter γ determines the magnitude of the energy gap $E_g\sim\Delta/(1+\gamma)$ in the spectrum of the horizontal lead (see below). The second term describes suppression of the condensate function v_N due to rapid change of the spectral phase across the tunnel barrier. This effect is similar to the mechanism which produces the Andreev bound states in the vicinity of the tunnel junction in the ballistic[23,5] as well as diffusive[31] Josephson structures. The third term is caused by the supercurrent flow through the normal lead. Neglecting this small $(\sim r^{-1})$ term, we obtain the solution of Eq. (29),

$$v_N=\frac{\tilde{\Delta}}{\sqrt{E^2-\tilde{\Delta}^2}},\quad \tilde{\Delta}(E,\phi)=\frac{\Delta_\phi}{1+\gamma\sqrt{\Delta^2-E^2}/\Delta}. \quad (31)$$

According to Eq. (31), the energy gap $E_g(\phi)$ in the spectrum of the junction is to be determined by the equation $E_g=|\tilde{\Delta}(E_g,\phi)|$, whose solution can be well approximated by a simple relation $E_g=|\Delta_\phi|/(1+\gamma)$.

Thus, the regime of strong proximity effect with the proximity gap being of the order of Δ [Fig. 3(a)] persists in short junction despite of high-resistive interfaces, $R_{NS}\gg R_N$, as long as the condition $\gamma\lesssim 1$ holds. In this case, the supercurrent spectral density

$$I_s(E,\phi)=-\operatorname{Im} I=-\frac{\sin(\phi/2)}{\sigma R_{NS}}\operatorname{Im}\left[\frac{\Delta v_N(E,\phi)}{\sqrt{E^2-\Delta^2}}\right] \quad (32)$$

extends over all quasiparticle states above the proximity gap, including the continuum states above the bulk energy gap Δ, where $I_s(E)$ is negative [Fig. 3(b)]. In the limit $\gamma\ll 1$ (recall that we nevertheless assume here the interface resistance to be large, $r\gg 1$), the dephasing effect becomes negligibly small and the energy gap approaches $|\Delta_\phi|$, similar to the perfect SNS junction discussed above. However, the shape of the supercurrent spectral density essentially differs from Eq. (25),

$$I_s(E)=\frac{\sin\phi}{2\sigma R_{NS}}\frac{\Delta^2\Theta(E-|\Delta_\phi|)\Theta(\Delta-E)}{\sqrt{E^2-\Delta_\phi^2}\sqrt{\Delta^2-E^2}}. \quad (33)$$

It is interesting to note that the expression for the equilibrium Josephson current obtained from Eq. (33),

$$j_s=\frac{\Delta\sin\phi}{2eR_{NS}}K(|\sin(\phi/2)|),\quad \gamma\ll 1\quad (T=0) \quad (34)$$

(K is the elliptic integral), can be reproduced with the arguments of the scattering theory, similar to the case of perfect diffusive SNS junction,[32] by applying the transmissivity distribution for a normal symmetric double-barrier structure.[33] Such a possibility is explained by the absence of electron-hole dephasing in this limit.

The proximity gap is strongly suppressed, $E_g\ll\Delta$, only in the limit of very large barrier strength, $\gamma\gg 1$.[17] This is the effect of enhanced electron-hole dephasing, similar to the case of a long diffusive SNS junction, where the proximity gap is also reduced due to the dephasing effect and closes at $\phi=\pi$. This situation is qualitatively different from the case of the tunnel junction with a single barrier, giving the Josephson current in junctions with two strong barriers,

$$j_s=\frac{\Delta\sin\phi}{2eR_{NS}\gamma}\ln\frac{4\gamma}{|\cos(\phi/2)|},\quad \gamma\gg 1\quad (T=0), \quad (35)$$

to be much smaller than the result of the tunnel model.[34]

IV. KINETIC EQUATIONS

In the absence of inelastic collisions, the kinetic equations in each lead have the form of conservation laws for the spectral currents $I_\pm(E)$,

$$D_\pm\partial f_\pm+I_s f_\mp\pm I_{an}\partial f_\mp\equiv I_\pm(E)=\text{const}. \quad (36)$$

At the junction node, the conservation law for the matrix currents in Eq. (3) imposes the boundary condition

$$I_\pm^L=I_\pm^R+I_\pm^V, \quad (37)$$

where the indices L, R, and V refer to the left, right, and injection leads, respectively. At the transparent interfaces, the distribution functions are determined by the local-equilibrium population in the reservoirs,

$$f_+(\pm d)=\tanh\frac{E}{2T}\quad (E>\Delta),\quad f_-(\pm d)=0, \quad (38a)$$

$$f_\pm(L)=n_\pm\equiv\frac{1}{2}\left[\tanh\frac{E+eV}{2T}\pm\tanh\frac{E-eV}{2T}\right]. \quad (38b)$$

At $E<\Delta$, the quasiparticle population in the leads is disconnected from the superconducting reservoirs due to complete Andreev reflection, and the quasiparticle density function f_+ is determined by the condition of the absence of the net probability current $I_+=0$. Due to the conservation law in Eq. (37), the subgap probability current I_+ turns to zero within the entire device.

In the energy region $E>\Delta$, where the currents I_s and I_{an} turn to zero, and the diffusion coefficient D_+ turns to unity, the kinetic equations have a simple solution,

$$I_+^R = \frac{n_0 - n_+}{R_+ + 2R_+^V}, \quad I_-^R = -\frac{n_-}{R_- + 2R_-^V}. \tag{39}$$

Here the quantities $R_+ = d$, $R_+^V = L$, $R_- = d\langle 1/D_-^{R,L}\rangle$, and $R_-^V = L\langle 1/D_-^V\rangle$ play the role of effective resistances of the leads for the spectral currents $I_\pm$, and the angle brackets denote spatial averaging along the leads. The currents in the left lead are equal by magnitude but flow in opposite directions, $I_\pm^L = -I_\pm^R$, and therefore the currents in the injection lead are twice the currents in the left lead. Combining this result with the relation $f_+(0) - n_0 = -R_+ I_+^R$, following from the kinetic equations, we find that in the limit of long injection lead the boundary condition at the junction node becomes independent of applied voltage,

$$f_+(0) = n_0, \quad L \gg d, \tag{40}$$

which implies that the quasiparticles in horizontal leads are in equilibrium with the superconducting reservoirs.

Within the subgap energy region, $E < \Delta$, the situation is more complex due to appearance of the currents I_s and I_{an}; the only simplification is due to the zero quasiparticle current $I_+ = 0$. By this reason, $f_+^V = \text{const} = n_+$ within the entire injection lead, including the junction node. Thus, the boundary conditions for the distribution functions in the horizontal leads read

$$f_+(0) = n_+, \quad f_-(0) = n_- - R_-^V I_-^V, \quad f_-(\pm d) = 0. \tag{41}$$

Taking advantage of the symmetry of the quantities $D_\pm(x) = D_\pm(-x)$ and $I_{an}(x) = -I_{an}(-x)$, we separate the even and odd parts of the distribution functions, $f^{s,a}(x) = [f(x) \pm f(-x)]/2$, in Eqs. (36), which then become split in the two independent pairs of kinetic equations. One pair that couples f_+^s and f_-^a,

$$D_+ \partial f_+^s + I_s f_-^a - I_{an} \partial f_-^a = 0, \tag{42a}$$

$$D_- \partial f_-^a + I_s f_+^s + I_{an} \partial f_+^s = (I_-^R + I_-^L)/2, \tag{42b}$$

has a constant solution, $f_+^s = n_+$, $f_-^a = 0$, consistent with the boundary conditions, which yields the relation $I_s n_+ = (I_-^R + I_-^L)/2$. As we will see later, Eq. (48), the nonequilibrium Josephson current j_s has the form $j_s = (j^R + j^L)/2$, and taking into account Eq. (4), we arrive at the following result:[35]

$$j_s = \frac{\sigma_N}{e} \int_0^\Delta dE\, I_s(E) n_+(E). \tag{43}$$

The second pair of kinetic equations couples the functions f_+^a and f_-^s,

$$D_+ \partial f_+^a + I_s f_-^s - I_{an} \partial f_-^s = 0, \tag{44a}$$

$$D_- \partial f_-^s + I_s f_+^a + I_{an} \partial f_+^a = -I_-^V/2. \tag{44b}$$

Since the source term and also the boundary conditions to these equations, Eq. (41), depend on I_-^V, these functions determine the dissipative current. The solution to Eq. (44) in general case must be found numerically.

At zero temperature, it is possible to further extend the analysis. By making use of a stepwise shape of the distribution functions $n_\pm = \Theta[\pm(E - eV)]$, we find that a trivial solution, $f_+^a = 0$, $f_-^s = 0$, $I_-^V = 0$, satisfies Eq. (44) and all the boundary conditions at $E > eV$. Thus the dissipative current vanishes in this energy interval. On the other hand, at $E < eV$, where $n_+ = 0$ and $n_- = 1$, Eqs. (44) have a nontrivial solution, which implies that the dissipative current exists at these energies, while the Josephson current is zero, according to Eq. (43). Thus at zero temperature the dissipative and nondissipative currents flow within the separate energy regions, which do not overlap: The injection current spreads over the energy region $0 < E < eV$,

$$j^V = \frac{\sigma_N}{e} \int_0^{eV} dE\, I_-^V(E), \tag{45}$$

while the supercurrent occupies the region $eV < E < \Delta$,

$$j_s = \Theta(\Delta - eV) \frac{\sigma_N}{e} \int_{eV}^\Delta dE\, I_s(E). \tag{46}$$

The analysis for the subgap region also applies to the case of resistive interfaces $r \gg 1$. However, at the energies $E > \Delta$, the supercurrent I_s and anomalous current I_{an} are nonzero and give additional contribution to the Josephson current in Eq. (46).

V. NONEQUILIBRIUM JOSEPHSON CURRENT

In equilibrium, the Josephson current is given by the second term in Eq. (5), as it was mentioned in Sec. II. Under nonequilibrium conditions, this connection becomes ambiguous and needs reconsideration. The reason is that the appearance of the dissipative currents and related gradients of the distribution functions in Eq. (5) will lead to spatial variation of the supercurrent term along the horizontal lead. To find an appropriate equation for the observable nonequilibrium Josephson current, we refer to a generic definition of the dc Josephson effect, as a current flow through a junction without any dissipation. In our case, the rate of the energy transfer from a voltage source to the junction is given by the equation

$$W = \int_{-d}^{d} dx\, j(x) \frac{dV}{dx} = j^L V^L + j^R V^R, \tag{47}$$

where $V^{L,R}$ are the voltage drops at the left/right leads. The stationary Josephson effect assumes zero voltage drop between the superconducting electrodes, $V^L + V^R = 0$, thus the nondissipative current component must satisfy the equation $j_s^L = j_s^R \equiv j_s$. Combining this equation with the Kirchhoff's rule, we arrive at the following definition of the Josephson current through the currents in the left, right, and injection leads,

$$j^{L,R} = j_s \pm j^V/2. \tag{48}$$

Thus, in order to evaluate observable Josephson current in a general case, it is necessary to calculate the injection current

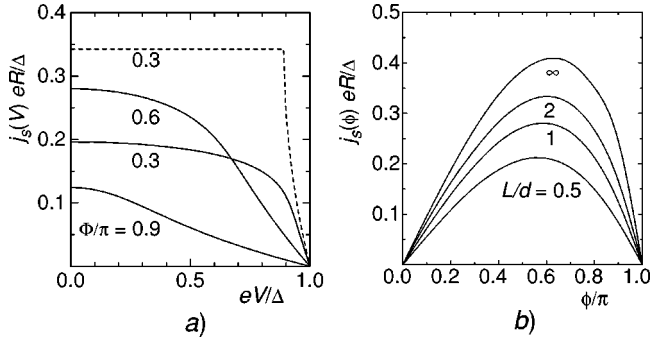

FIG. 4. Josephson current vs voltage at different phases: solid lines represent $L=d$ and dashed line represents $L\gg d$ (a), and Josephson current vs phase at several values of the ratio L/d (b).

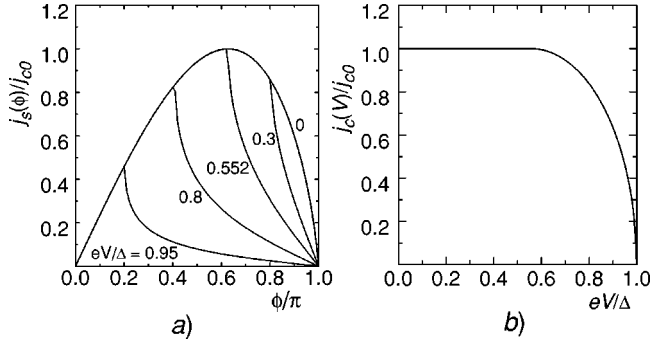

FIG. 5. Current-phase relations from Eq. (50) at different voltage (a), and critical current vs voltage (b) at $L\gg d$. For a given voltage, the current-phase relation follows the equilibrium law as soon as the proximity gap edge is above the energy eV, but it is significantly suppressed when the gap edge is below eV.

and the current in one of the horizontal leads, and then apply Eq. (48). In particular case of symmetric junction, this procedure leads to Eq. (43).

Persistent current in a SQUID is the most fundamental manifestation of the Josephson effect. The Josephson current in Eq. (48) coincides with the circulating current, and it can be directly measured by measuring the induced flux with an external magnetometer.

Let us first consider junctions with transparent interfaces, where the nonequilibrium Josephson current is given by Eq. (46). Since the spectral density I_s is positive in this case, as it is found from numerical solution of Eq. (23), and the population of the subgap states is depleted with increasing voltage, the injection will suppress the Josephson current and block it completely at $eV>\Delta$ [see Fig. 4(a)]; however, the current direction cannot be reversed. The Josephson current weakly depends on the applied voltage and is close to the equilibrium value as long as the voltage is smaller than the proximity gap value, $eV<|\Delta_\phi|$. We note that this equilibrium value differs from that in closed SNS junctions,[36] it is reduced due to the proximity of the normal reservoir and therefore depends on the length of the injection lead, as shown in Fig. 4(b). At larger voltage, the Josephson current-voltage dependence $j_s(V)$ becomes more steep, especially for the small phase differences.

For a long injection lead, Eq. (46) takes the form

$$j_s(\phi,V)=\frac{\pi\Delta_\phi}{2eR_N}\int_{|\Delta_\phi|}^{\Delta}dE\,\frac{n_+(E)}{\sqrt{E^2-\Delta_\phi^2}}. \qquad (49)$$

At zero temperature, the integration in Eq. (49) can be explicitly performed,[20]

$$j_s(\phi,V)=\frac{\pi\Delta_\phi}{2eR_N}\ln\frac{1+\sin(\phi/2)}{f(V)+\sqrt{f^2(V)-\cos^2(\phi/2)}}, \qquad (50)$$

$$f(V)=\max[eV/\Delta,\cos(\phi/2)], \quad eV>|\Delta_\phi|. \qquad (51)$$

This current-voltage dependence is shown in Fig. 4(a) by a dashed line. In this case, the Josephson current at $eV<|\Delta_\phi|$ is constant and equal to the equilibrium value.

To estimate the efficiency of the Josephson transistor, let us consider the most steep part of the current-voltage characteristic, $j_s(\phi,V)$, at small phase and at large voltage. For example, at $\phi=0.3\pi$, when the equilibrium Josephson current approaches about 0.7 of its critical value j_c, the switching effect occurs within a small voltage interval $\delta V\sim 0.1\Delta/e$. The current gain in this case, $\delta j_s/\delta j^V\sim 0.7 j_c/G\,\delta V\sim 7(L/d)$, exceeds unity even for comparable lengths of the leads, and it can be further enhanced by making the injection lead longer. The upper bound for the gain is imposed by the condition of small quasiparticle dwelling time $L^2/\mathcal{D}$, compared to the quasiparticle relaxation time τ, $L^2/\mathcal{D}\ll\tau$.

The nonequilibrium Josephson current-phase dependence for the junctions with transparent interfaces and high-resistive injection lead is shown in Fig. 5(a) for different applied voltages. The kinks on the graphs correspond to the phase values, at which the applied voltage equals the proximity gap, $\phi_0(V)=2\arccos(eV/\Delta)$. At smaller phases, $0<\phi<\phi_0(V)$, the current-phase dependence has an equilibrium form, while at larger phases it is considerably distorted. Correspondingly, the critical current $j_c(V)$ remains independent of applied voltage until $\phi_0(V)$ exceeds the value $\phi_m=1.97$, at which the equilibrium supercurrent approaches its maximum value $j_{c0}=j_c(0)=0.66\pi\Delta/2eR$. At larger voltage, $eV>\Delta\cos(\phi_m/2)=0.55\Delta$, the critical current decreases and turns to zero at $eV\gtrsim\Delta$, as shown in Fig. 5(b),

$$\frac{j_c(V)}{j_c(0)}=\frac{j_s[\phi_0(V),0]}{j_c(0)}=1.51\frac{eV}{\Delta}\,\mathrm{arccosh}\frac{\Delta}{eV}. \qquad (52)$$

In junctions with resistive interfaces, $r\gg 1$, the current-phase dependence is more interesting, because of the possibility of the Josephson current inversion and the crossover to the π-junction regime. This results from the negative contribution of the energies $E>\Delta$ to the Josephson current which turns to zero before the voltage achieves the gap value, $eV\lesssim\Delta$, when the positive and negative parts of $I_s(E)$ compensate each other. At larger voltage the current becomes negative, as shown in Fig. 6(a). Detailed analysis of the crossover region can be made for the junctions with high-resistive injection lead, $L/d\gg r\gg 1$, and at zero temperature. In this case, in the horizontal leads, the distribution function f_- is

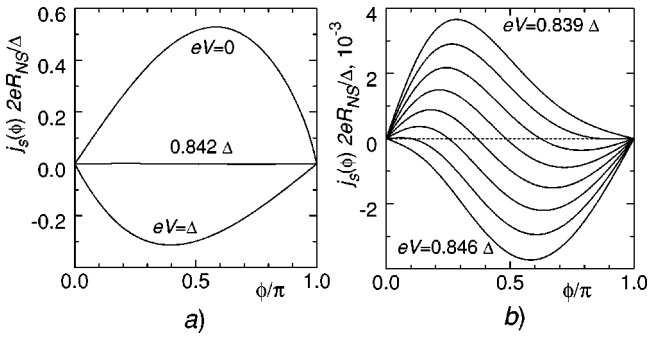

FIG. 6. Inversion of the current-phase relation $j_s(\phi)$ under applied voltage in a SINIS junction at $\gamma=1$. The voltage step between the curves in right panel is $10^{-3}\Delta/e$.

small, and the function f_+ is approximately constant and approaches the equilibrium value $n_0(E)=1$ in the superconducting reservoir [see Eq. (40)]. By these reasons, the small dissipative and anomalous components can be omitted from the current spectral density $I_-\approx I_s$, which then becomes independent of the applied voltage at $eV>\Delta$. This results in the following modification of Eq. (46):

$$j_s=\frac{\sigma}{e}\int_{min(eV,\Delta)}^{\infty} dE\, I_s(E), \tag{53}$$

where $I_s(E)$ is to be found from Eqs. (32) and (31).

As follows from Eq. (53), the critical voltage at which the current turns to zero depends on the phase, and therefore the crossover extends over a certain (in fact, rather small), voltage interval, as shown in Fig. 6(b). When the voltage approaches the critical region, a new current node in the current-phase dependence splits from the node at $\phi=\pi$, then it moves towards smaller ϕ; the process ends where the extra node approaches $\phi=0$. Such a fine structure of the Josephson current inversion has been observed experimentally in long SNS junctions.[11] At very large interface resistance, $\gamma \gg 1$, this fine structure becomes irresolvable because of the fact that in this limit the phase dependence in $I_s(E,\phi)$ for relevant energies is given by a prefactor $\sin\phi$, and therefore the compensation effect appears simultaneously at all phases.[17]

VI. CRITICAL CURRENT IN CURRENT BIASED JUNCTION

In experiment, the current bias setup is often employed for investigation of the dc Josephson current, Fig. 1(c). In equilibrium, the maximum value of the current flowing through the junction without creating a voltage drop coincides with the maximum current in the current-phase dependence. This is not the case for a nonequilibrium junction with current injection: the ''critical'' current is contributed by both the nonequilibrium Josephson current and the injection current.

Suppose the voltage is applied between the injection electrode and left superconducting electrode, Fig. 1(c), then the external transport current j_T is equal to the current j^R in the right lead. In this case, the problem of the critical current

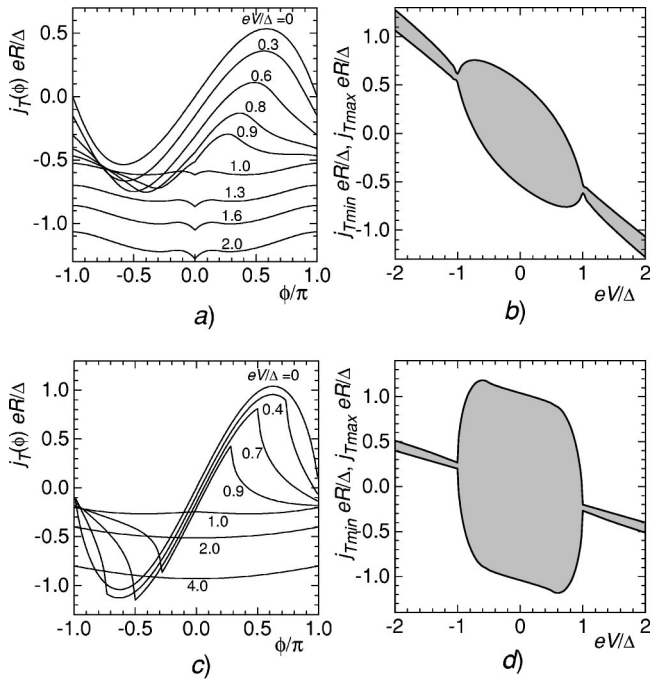

FIG. 7. Current j_T vs phase ϕ at different injection voltages (a,c), and critical transport current j_{Tmin}, j_{Tmax} vs voltage (b,d), at $L=d$ (a,b), and $L=5d$ (c,d). Shaded regions correspond to zero potential difference between the superconducting electrodes. In oval-like regions, the Josephson current coexists with the normal current; in shaded stripes at $eV>\Delta$, the Josephson current is absent (Josephsonlike regime).

evaluation is reduced to the analysis of the phase dependence of $j^R=j_s-j^V/2$ at a given voltage. The requirement of zero potential difference between the superconducting electrodes is automatically fulfilled in our calculation (time-independent phase difference). For simplicity, we consider the junction with perfect interfaces, where the currents are given by Eqs. (45) and (46).

The numerical results of such analysis are shown in Fig. 7(a,c). They are obtained by solving numerically Eq. (23) for the spectral functions and Eq. (36) for the distribution functions, which determine the magnitude of the injection current. At $eV<\Delta$, when the supercurrent is allowed to flow through the junction, the current-phase relations are similar to that depicted in Fig. 5(a). At these voltages, the Josephson current coexists with the normal current flowing out of the injection lead. At larger voltages, $eV>\Delta$, the supercurrent is blocked, however, the transport current still flows through the junction without voltage drop across it, within a certain range of the current magnitudes determined by the amplitude of the dependence $j^R(\phi)$. The existence of such Josephson-like regime without real Josephson current has been first pointed out for a four-terminal SNS junction with opaque interfaces.[6]

To understand this phenomenon, it is important to remember that the injection current in NS interferometers is not uniquely determined by the bias voltage, but also depends on the superconducting phase. In principle, a similar regime with zero voltage drop across the junction may appear even for normal reservoirs, at the transport current $j_T=j^V(V)/2$.

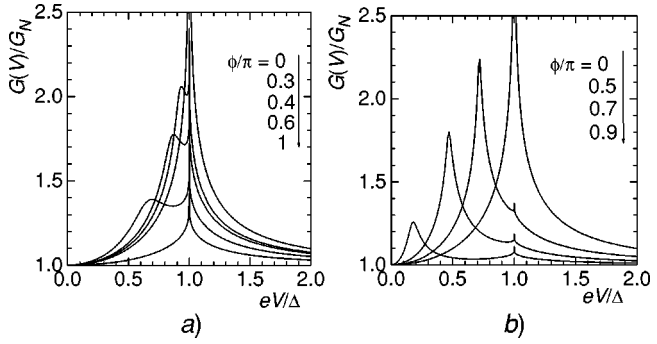

FIG. 8. Differential conductance G vs voltage at $L=d$ (a) and $L=5d$ (b) for different phases.

This value is unique for the given injection voltage, and therefore the corresponding dependence $j_T(V)$ is represented by a straight line. In the superconducting junctions, such line broadens to a stripe, $j_T=j^V(V,\phi)/2$, due to the presence of the free parameter ϕ: The phase adjusts the injection current for given injection voltage and transport current to provide zero voltage drop across the junction. The width of the stripe is determined by the amplitude of the injection current oscillation with the phase. At $eV<\Delta$, this effect is hidden by the presence of the true supercurrent [large shaded regions in Figs. 7(b,d)], however, it is fully revealed at $eV>\Delta$, where the supercurrent is suppressed [shaded stripes in Figs. 7(b,d)]. In fact, at large voltage, the width of the shaded stripes is determined by the amplitude of phase oscillations of the excess injection current. The qualitative difference between the phase dependence of the excess current ($eV>\Delta$) and the Josephson current ($eV<\Delta$) is clearly seen in Figs. 7(a,c). It is interesting that the ''critical current'' has different sign for positive and negative voltages [the shaded stripes in Fig. 7(b,d) are differently oriented with respect to the straight line]. This is consistent with the fact that the excess current changes sign along with the applied voltage.

VII. INTERFEROMETER EFFECT

In this section, we investigate the conductance of the injection lead as a function of the bias voltage and superconducting phase focusing on its properties due to the strong proximity effect. At small temperatures, $T\ll eV$, the overall voltage dependence of the differential conductance is given by Eq. (45), $G(V,\phi)=dj^V/dV=\sigma I_-^V$, where the injection current I_-^V is to be calculated by numerical solution of Eq. (23) for the spectral functions and the kinetic equations (36). As shown in Fig. 8, the conductance has two peaks, at voltages $eV=\Delta$ and $eV\approx|\Delta_\phi|$. The first peak is associated with enhanced transmissivity of the junction due to the DOS peak at the bulk gap edge. This peak has a logarithmic singularity at $\phi=0$, and it becomes smeared and decreases while ϕ departs from zero. The second peak manifests a rapid change in the spectral functions in the vicinity of the spectrum edge in a short SNS junction (see Fig. 2), and it can be interpreted as a resonance transmission due to enhanced DOS at the proximity gap edge $|\Delta_\phi|$. As soon as L increases, this resonance becomes more sharp because the singularities in the spectral functions at $E=|\Delta_\phi|$ become more pronounced, whereas the peak at the bulk gap edge, $eV=\Delta$, decreases and vanishes at $d/L\to 0$, as shown in Fig. 8(b). Furthermore, the conductance exhibits the reentrance effect: $G(V)$ approaches the value $G_N=\sigma/(d/2+L)$ in the normal state both at small and large voltages, as it was predicted for NS point contacts.[37] We notice that the differential conductance $G(V)$ deviates from G_N in the short-arm interferometers at the characteristic energy of the order of Δ, in contrast to the long-arm SNS junctions ($d\gg\xi_0$), where the conductance peak appears at the Thouless energy $E_{\rm Th}=\hbar\mathcal{D}/(2d)^2\ll\Delta$.[38]

At zero phase difference, $\phi=0$, the function $G(V)$ can be found analytically. In this case, $I_s=I_{an}=0$, and the function f_- obeys a simple equation $D_-\partial f_-=I_-$ in each lead, with the diffusion coefficients

$$D_-^{R,L}=\cosh^2\left[\mathrm{Re}\,\theta_S(E)\,\frac{1+a|x|/d}{1+a}\right], \tag{54a}$$

$$D_-^V=\cosh^2\left[\mathrm{Re}\,\theta_S(E)\,\frac{1-y/L}{1+a}\right]. \tag{54b}$$

From Eqs. (45) and (54), we obtain

$$G(V)=G_N\eta(eV)\quad(\phi=0), \tag{55}$$

$$\eta(E)=z\,\mathrm{arctanh}\,z^{-1},\quad z=(E/\Delta)^{\mathrm{sgn}(E-\Delta)}. \tag{56}$$

The oscillations of the conductance peak at $eV=\Delta$ with the phase can be found from the following arguments. At this energy, the diffusion coefficient D_- turns to infinity in the horizontal lead, which therefore becomes nonresistive with respect to the normal current, $R_-(\Delta)=0$. Thus, the differential conductance at $eV=\Delta$ is completely determined by the resistance of the injection lead $[R_-^V(\Delta)=L\tanh\theta_0/\theta_0]$, where $\theta_0=\ln\cot(\phi/4)$,

$$G_{\max}(\phi)\equiv G(\Delta/e,\phi)=G_N\frac{1+a}{\cos(\phi/2)}\ln\cot\frac{\phi}{4}. \tag{57}$$

According to Eq. (57), the peak height approaches $G_N(1+a)$ at $\phi=\pi$. At this point, like at $\phi=0$, the spectral densities of the superconducting and anomalous current turn to zero, and only the resistances R_- and R_-^V are involved in the calculation. Since the condensate function becomes completely suppressed in the middle of the junction, $\theta_0=0$, the injection lead behaves as a normal wire, and therefore the resistance R_-^V approaches its normal value L. Correspondingly, the resistance of each horizontal lead coincides with the resistance of a short NS junction with the length d, $R_-=d\tanh(\mathrm{Re}\,\theta_S)/\mathrm{Re}\,\theta_S$, and therefore $G(V)$ at $\phi=\pi$ is given by

$$G(V)=G_N\frac{1+a}{1+a/\eta(eV)}\quad(\phi=\pi). \tag{58}$$

In the limit of long injection lead, $d/L\to 0$, its resistance $R_-^V=L\tanh\mathrm{Re}\,\theta_0/\mathrm{Re}\,\theta_0$, $\theta_0=\mathrm{arctanh}(\Delta_\phi/E)$ completely determines the injection current, and the voltage dependence

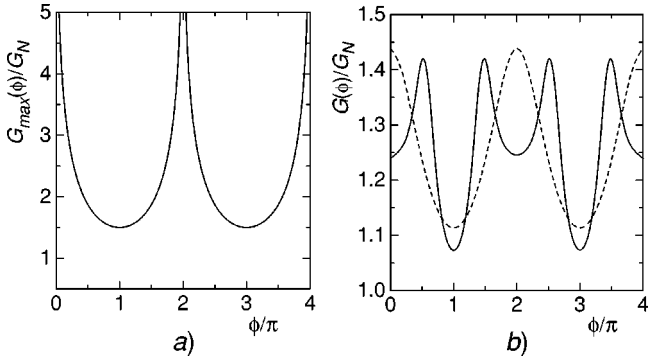

FIG. 9. Differential conductance vs phase at $L=d$ and different voltage: $V=\Delta/e$ (a), $V=0.7\Delta/e$ [(b), solid line], and $V=1.2\Delta/e$ [(b), dashed line].

of the differential conductance shown in Fig. 8(b) is approximately described by Eq. (55), with $|\Delta_\phi|$ substituted for Δ in the function $\eta(eV)$.

The differential conductance exhibits full-scale 2π-periodic oscillations with the phase difference ϕ (Andreev interferometer effect). The form of the oscillations is qualitatively different for the subgap bias region, $eV<\Delta$, and for $eV>\Delta$, as shown in Fig. 9(b). In the latter case, the phase dependence of G has a comparatively simple form, with maxima at $\phi=2\pi n$ and minima at $\phi=(2n+1)\pi$. At $eV<\Delta$, the differential conductance approaches minima both at even and odd multiples of π, which reflects the interplay between the position and amplitude of the resonance at $eV=|\Delta_\phi|$.

VIII. SUMMARY

We have developed a theory of the nonequilibrium Josephson effect in a three-terminal diffusive interferometer with short SNS junction having the length $2d$ much smaller than the superconducting coherence length ξ_0. We focused on the case of strong proximity effect, when the proximity energy gap in the normal region is of the order of Δ. For the junction with transmissive NS interfaces, the density of states, $N(E)$, and the supercurrent spectral density $I_s(E)$ extend over the whole subgap region, $0<E<\Delta$, due to the proximity to a normal reservoir, and exhibit a considerable enhancement at the energy equal to the proximity gap $|\Delta_\phi|=\Delta|\cos(\phi/2)|$ in the spectrum of a closed SNS junction. The supercurrent spectral density is positive at all relevant energies. We demonstrated a possibility of the strong proximity effect in a junction with opaque interfaces whose resistance R_{NS} is much larger than the normal resistance R_N of the junction arms. In such case, the suppression of the proximity gap $E_g(\phi)\approx|\Delta_\phi|/(1+\gamma)$ is controlled by the parameter $\gamma=(2R_{NS}/R_N)(d/\xi_0)^2$, which could be small in short junctions, $d\ll\xi_0$, even at large interface resistance, $R_{NS}\gg R_N$. In contrast to the case of transmissive interfaces, the supercurrent spectral density $I_s(E)$ is negative above the bulk gap value.

In three-terminal interferometers, the supercurrent generally coexists with the dissipative current flowing out from the injection electrode. In such situation, we defined the nonequilibrium Josephson current j_s as the nondissipative component of the current flowing between the superconducting electrodes. In symmetric junctions, within the subgap energy region, this component coincides with its intuitive representation through the supercurrent spectral density I_s and the quasiparticle population imposed by nonequilibrium injection, because the Andreev reflection blocks quasiparticle exchange with equilibrium superconducting reservoirs. In junctions with transmissive interfaces the Josephson current becomes completely blocked at $eV=\Delta$ at zero temperature, while in junctions with high-resistive interfaces, the Josephson current undergoes inversion at $eV\lesssim\Delta$, which spreads over a finite voltage interval. At the energies above the bulk energy gap, $E>\Delta$, the population in the junction arms is basically determined by the equilibrium population in the superconducting reservoirs. By this reason, the Josephson current becomes voltage independent at $eV>\Delta$.

We notice that spectroscopy of the supercurrent spectral density at the subgap energies is possible at zero temperature, similar to the tunnel spectroscopy of $N(E)$, because the derivative of the Josephson current over applied voltage, dj_s/dV, is proportional to $I_s(eV)$.

The critical current j_c of the three-terminal junction, defined as the maximum value of the transport current j_T flowing through the junction without creating a voltage drop, does not coincide with the maximum in $j_s(\phi)$. This is due to the presence of phase-dependent injection current $j^V(\phi)$ which contributes to j_c, along with the Josephson current, and adjusts its magnitude providing zero voltage drop across the junction. At large voltage, where the Josephson current is suppressed, the domain of the Josephson-like regime is determined by the amplitude of phase oscillations of the excess current in the injection electrode.

The behavior of the injection current is highly sensitive to the quasiparticle spectrum of the junction and can be used to detect the position of the phase-dependent proximity gap. In particular, the differential conductance of the junction with perfect interfaces exhibits sharp peaks at the bulk gap value, $eV=\Delta$, and at the proximity gap, $eV=|\Delta_\phi|$; the latter becomes more pronounced as the resistance of the injection lead increases. Furthermore, the differential resistance exhibits full-scale oscillations with the phase difference; at $eV<\Delta$, the shape of the oscillations becomes rather complex, due to the interplay between the position and amplitude of the proximity gap resonance.

ACKNOWLEDGMENTS

Support from VR and KVA (Sweden) is gratefully acknowledged.

[1] C.J. Lambert and R. Raimondi, J. Phys.: Condens. Matter **10**, 901 (1998).
[2] P. Samuelsson, J. Lantz, V.S. Shumeiko, and G. Wendin, Phys. Rev. B **62**, 1319 (2000).
[3] F.W.J. Hekking and Yu.V. Nazarov, Phys. Rev. Lett. **71**, 1625 (1993); H. Nakano and H. Takayanagi, Phys. Rev. B **47**, 7986 (1993).
[4] B.J. van Wees, K.M.H. Lenssen, and C.J.P.M. Harmans, Phys. Rev. B **44**, 470 (1991).
[5] G. Wendin and V.S. Shumeiko, Phys. Rev. B **53**, R6006 (1996).
[6] A.F. Volkov and V.V. Pavlovskiĭ, JETP Lett. **64**, 670 (1996).
[7] A.F. Volkov and H. Takayanagi, Phys. Rev. Lett. **76**, 4026 (1996); Phys. Rev. B **56**, 11 184 (1997); R. Shaikhaidarov, A.F. Volkov, H. Takayanagi, V.T. Petrashov, and P. Delsing, *ibid.* **62**, R14 649 (2000).
[8] V.T. Petrashov, V.N. Antonov, P. Delsing, and T. Claeson, Phys. Rev. Lett. **70**, 347 (1993); P.G.N. de Vegvar, T.A. Fulton, W.H. Malinson, and R.E. Miller, *ibid.* **73**, 1416 (1994); H. Pothier, S. Gueron, D. Esteve, and M.H. Devoret, *ibid.* **73**, 2488 (1994).
[9] A.F. Volkov and A.V. Zaitsev, Phys. Rev. B **53**, 9267 (1996); A.V. Zaitsev, A.F. Volkov, S.W.D. Bailey, and C.J. Lambert, *ibid.* **60**, 3559 (1999).
[10] A.F. Morpurgo, T.M. Klapwijk, and B.J. van Wees, Appl. Phys. Lett. **72**, 966 (1998); J.J.A. Baselmans, A.F. Morpurgo, B.J. van Wees, and T.M. Klapwijk, Nature (London) **397**, 43 (1999).
[11] J.J.A. Baselmans, T.T. Heikkilä, B.J. van Wees, and T.M. Klapwijk, Phys. Rev. Lett. **89**, 207002 (2002).
[12] J. Huang, F. Pierre, T.T. Heikkilä, F.K. Wilhelm, and N.O. Birge, Phys. Rev. B **66**, 020507(R) (2002).
[13] P. Samuelsson, V.S. Shumeiko, and G. Wendin, Phys. Rev. B **56**, R5763 (1997).
[14] L.F. Chang and P.F. Bagwell, Phys. Rev. B **55**, 12 678 (1997).
[15] P. Samuelsson, Å. Ingerman, V. Shumeiko, and G. Wendin, Physica C **352**, 82 (2001).
[16] A.F. Andreev, Zh. Eksp. Teor. Fiz. **46**, 1823 (1964) [Sov. Phys. JETP **19**, 1228 (1964)].
[17] A.F. Volkov, Phys. Rev. Lett. **74**, 4730 (1995).
[18] F.K. Wilhelm, G. Schön, and A.D. Zaikin, Phys. Rev. Lett. **81**, 1682 (1998).
[19] S.K. Yip, Phys. Rev. B **58**, 5803 (1998).
[20] T.T. Heikkilä, J. Särkkä, and F.K. Wilhelm, Phys. Rev. B **66**, 184513 (2002).
[21] A.F. Volkov and T.M. Klapwijk, Phys. Lett. A **168**, 217 (1992); A.F. Volkov, A.V. Zaitsev, and T.M. Klapwijk, Physica C **210**, 21 (1993).
[22] R. Seviour and A.F. Volkov, Phys. Rev. B **61**, 9273 (2000).
[23] A. Furusaki and M. Tsukada, Phys. Rev. B **43**, 10 164 (1991).
[24] A.Yu. Kazumov, I.I. Khodos, P.M. Aiayan, and C. Colliex, Europhys. Lett. **34**, 429 (1996); A. Bezryadin, C.N. Lau, and M. Tinkham, Nature (London) **404**, 971 (2000).
[25] A.I. Larkin and Yu.N. Ovchinnikov, Zh. Eksp. Teor. Fiz. **68**, 1915 (1975) [Sov. Phys. JETP **41**, 960 (1975)]; **73**, 299 (1977) [**46**, 155 (1977)].
[26] Yu.V. Nazarov, Phys. Rev. Lett. **73**, 1420 (1994); Superlattices Microstruct. **25**, 1221 (1999).
[27] K.D. Usadel, Phys. Rev. Lett. **25**, 507 (1970).
[28] Similar solution for a diffusive point contact between superconductors was found in Ref. 36 by Matsubara technique.
[29] To next order, one should take into account the electron-hole dephasing at finite energy [second term in the rhs of Eq. (15)], which results in a small contribution to the supercurrent from the continuum states, $E>\Delta$, where the spectral density $I_s(E)$ is negative, Refs. 19,20.
[30] M.Yu. Kupriyanov and V.F. Lukichev, Zh. Eksp. Teor. Fiz. **95**, 159 (1988) [Sov. Phys. JETP **67**, 89 (1988)].
[31] E.V. Bezuglyi, E.N. Bratus', and V.P. Galaiko, Low Temp. Phys. **25**, 167 (1999).
[32] C.W.J. Beenakker, Phys. Rev. Lett. **67**, 3836 (1991); **68**, 1442 (1992).
[33] M.J.M. de Jong, Phys. Rev. B **54**, 8144 (1996).
[34] V. Ambegaokar and A. Baratoff, Phys. Rev. Lett. **10**, 486 (1963).
[35] Similar formula has been applied for calculation of the Josephson current in Ref. 12.
[36] I.O. Kulik and A.N. Omelyanchouk, JETP Lett. **21**, 96 (1975).
[37] S.N. Artemenko, A.F. Volkov, and A.V. Zaitsev, Solid State Commun. **30**, 771 (1979).
[38] Yu.N. Nazarov and T.H. Stoof, Phys. Rev. Lett. **76**, 823 (1996); A.F. Volkov, N. Allsopp, and C.J. Lambert, J. Phys. Condens. Matter **8**, 45 (1996); A.A. Golubov, F.K. Wilhelm, and A.D. Zaikin, Phys. Rev. B **55**, 1123 (1997).